Journal of Colloid and Interface Science 667 (2024) 563–574

Contents lists available at ScienceDirect

Journal of Colloid And Interface Science

journal homepage: www.elsevier.com/locate/jcis

Regular Article

Size, shape, and stability of organic particles formed during freeze–thaw cycles: Model experiments with tannic acid

Stefan Dultz [a,*], Myriam Speth [a,b], Klaus Kaiser [c], Robert Mikutta [c], Georg Guggenberger [a]

[a] Institute of Earth System Sciences, Section Soil Science, Leibniz Universität Hannover, Herrenhäuser Str. 2, 30419 Hannover, Germany
[b] Department of Soil Science and Soil Conservation, Justus Liebig Universität Giessen, Heinrich-Buff-Ring 26-32, 35392 Giessen, Germany
[c] Soil Science and Soil Protection, Martin Luther University Halle-Wittenberg, Von-Seckendorff-Platz 3, 06120 Halle (Saale), Germany

GRAPHICAL ABSTRACT

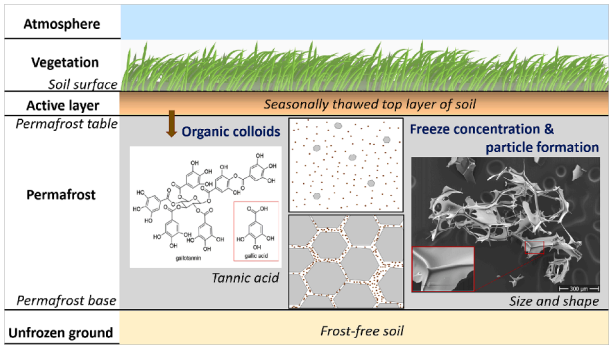

ARTICLE INFO

Keywords:
Self-aggregation
Freeze-concentration
Ice exclusion
Particle shape
Equivalent circle diameter
Hydrodynamic diameter
Particle stability

ABSTRACT

Hypothesis: Freeze-thaw cycles (FTC) in soils can cause the aggregation of dissolved organic matter but controlling factors are little understood.
Experiments: In freeze–thaw experiments with tannic acid (TA) as model substance, we studied the effect of TA concentration, pH, electrolytes (NaCl, $CaCl_2$, $AlCl_3$), and number of FTC on particle formation. Tannic acid (0.005 to 10 g L^{-1}) was exposed to 1–20 FTC at pH 3 and 6. The size and shape of particles was determined by confocal laser scanning microscopy. Particle stability was deduced from the equivalent circle diameter (ECD) obtained in dry state and the hydrodynamic diameter measured in thawing solutions.
Findings: Tannic acid particles occurred as plates and veins, resembling the morphology of ice grain boundaries. Low pH and presence of electrolytes favored the formation of large particles. The freeze-concentration effect was most intense at low TA concentrations and increased with the number of FTC. While ECD of particles formed at low TA concentrations were smaller than at high concentrations, it was *vice versa* in the thawed state. At low TA concentrations, higher crystallization pressure of ice caused enhanced stability of large particles. We conclude that FTC can strongly alter the physical state of dissolved organic matter, with likely consequences for its bioavailability.

* Corresponding author.
E-mail address: dultz@ifbk.uni-hannover.de (S. Dultz).

https://doi.org/10.1016/j.jcis.2024.04.080
Received 17 November 2023; Received in revised form 11 April 2024; Accepted 12 April 2024
Available online 16 April 2024

1. Introduction

Due to climate change permafrost degrades worldwide through the gradual deepening of the seasonal active layer and thermokarst formation [1], rendering soil organic carbon vulnerable to mobilization [2]. Climate change also leads to higher frequencies of freezing and thawing cycles (FTC) in high latitudes [3]. Freezing and thawing cycles may break down large organic and organic–mineral colloids into smaller-sized entities [4]. Likewise, FTC affect soil structure as ice pressure can cause either formation of aggregates from clay-sized particles or induce fragmentation of soil particles [5], thereby changing soil porosity and connectivity [6]. Higher frequencies of FTC have been reported to physically damage — soil aggregates, as well as cell membranes of microorganisms and fine roots, thus increasing the release of organic matter from soil as dissolved organic matter (DOM) and CO_2 [7–9].

Besides the physical effect of growing ice crystals on organic and inorganic particles, the "freeze-concentration effect" is another process that strongly affects particle growth during freezing, leading to the formation of larger organic molecules [10,11] or mineral–organic composites [12]. During water freezing, all non-aqueous components such as cations and anions, including H^+ and OH^-, organic molecules, mineral colloids, and air bubbles become concentrated in the residual liquid volume, a process known as freeze-concentration (Fig. 1), [11–14].

Ice crystallization reduces the energetic state by releasing crystallization energy, whereby solutes and solid particles act as impurities and do not fit in a crystal structure aspiring the lowest energetic state [12]. If particles are small compared to the ice crystal and move by Brownian motion, the solutes are excluded from the growing ice crystals and become concentrated at the freezing interface. With progressive growth of ice crystals, the residual liquid becomes increasingly concentrated since solutes and particles are captured at the outer surface of ice crystals. Particles excluded from the growing ice crystals are located at sub-grain boundaries (low-angle grain boundaries with a misorientation $< 15°$ between two crystallites), revealing forms with shapes of layers and veins forming at two- and three-grain boundaries, respectively [15–17]. The freeze-concentration process is known also for other systems, e.g., triggered by the solidification of an oil phase [18].

Since salt exclusion from the ice leads to an increase in salinity, freeze-concentrated solutions can substantially depress the freezing point and unfrozen water contents [19]. Freeze-concentrated solutions act as important reaction media, whereby their morphology is accessible by, e.g., optical cryo-microscopy and laser confocal fluorescence microscopy [20,21]. During freeze-concentration, dissolved compounds can selectively be incorporated into the ice, thus, affecting the freeze-concentrated solution composition. In rivers and lakes, low-molecular weight molecules are preferentially retained within the ice while more complex solutes are excluded [22]. Among inorganic ions, Cl^- is preferentially trapped within ice leading to a measurable charge separation, while Na^+ accumulates in freeze-concentrated solution [23,24].

In thermokarst lakes, freeze-driven solute concentration promotes particle formation by the coagulation of dissolved and colloidal organic molecules as well as precipitation of associated insoluble metal compounds [4,25]. Since an even stronger exclusion was observed for organic colloids than for electrolytes in aquatic systems [22], it can be assumed that also in soil freeze-concentration causes organic particle formation from organic solutes and colloids by exclusion from growing ice. We speculate that in soils, organic particles formed by freeze-concentration at high crystallization pressure can be physically stable and accumulate, e.g., as building units for soil microaggregates. Unlike rigid mineral particles, organic colloids have a more flexible structure and undergo marked losses of volume upon freezing. In consequence, organic particles will likely adapt in shape and size to sub-grain boundaries of the formed ice crystals. However, little is known about the behavior of organic solutes and colloids during this process.

The main objective of this study was to explore the consequences of FTC on the formation of particles from organic colloids in presence of different background electrolytes. We used tannic acid (TA) as model substance for DOM rich in phenolic compounds (i.e. hydrolysable gallotannin) [26]. Tannic acid is commonly found in DOM of soils and aquatic systems [27,28], with TA-type molecules representing up to 27 and 70 % of DOM in O horizons of pine and beech forests, respectively [29]. Conducting FTC using different concentrations of TA, pH values, and background electrolytes (without, NaCl, $CaCl_2$, $AlCl_3$), we aimed to

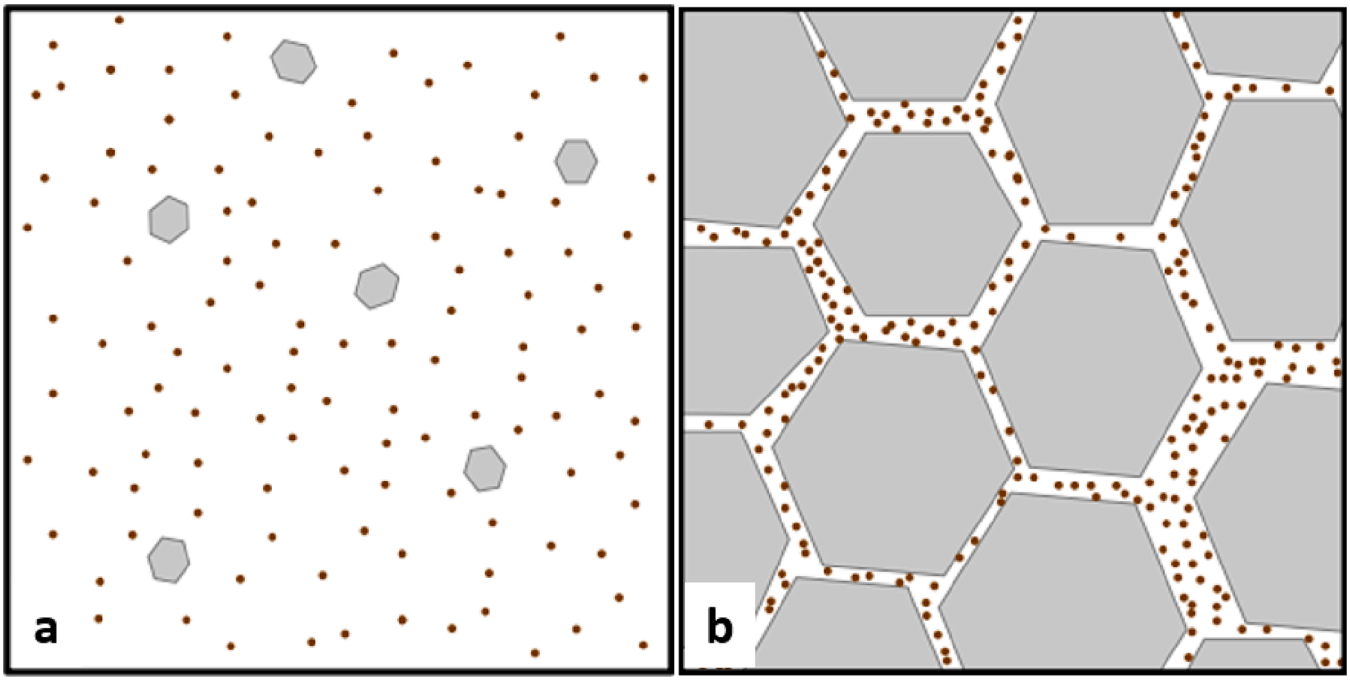

Fig. 1. Model of freeze-concentration at homogeneous temperature distribution. (a) After nucleation, ice begins to grow in a hexagonal system. (b) Growing ice crystals exclude impurities, which are concentrated in the residual liquid until its eutectic mixture is reached.

address the following hypotheses: (i) freezing at low TA concentrations results in larger particles due to larger ice crystals formed, (ii) repeated FTC amplify the size of TA particles, (iii) large freezing cross-sections result in formation of larger particles as the volume of the freeze-concentrated solution increases, (iv) low pH enhances the self-aggregation of TA upon freeze-concentration and favors formation of larger particles, and (v) multivalent cations support the self-aggregation process and increase the stability of particles formed. The morphology and equivalent circle diameter (ECD) of particles formed were analyzed by confocal laser scanning microscopy (CLSM) and scanning electron microscopy (SEM). Additionally, the hydrodynamic diameter (D_h) of TA particles released into solution at the end of FTC was determined by dynamic light scattering (DLS), allowing to compare particle formation in the solid and solution state, respectively.

2. Material and methods

2.1. Preparation of tannic acid solutions

Tannic acid powder was obtained from Riedel-de Haen (Seelze, Germany). The C and N content was 48.4 and 0.11 %, respectively (CN analyzer Vario EL, Elementar, Hanau, Germany) and the ignition residue $\leq$ 0.1 %. The used TA consists of gallic acid groups linked to a glucose core, forming hydrolysable gallotannin (AFig. 1). Considering the molecular weights of the protonated gallotannin (1700 g mol^{-1}) and gallic acid (170.1 g mol^{-1}), the mean degree of polymerization is 10, corresponding to higher polymerized TA. Stock solutions with a TA concentration of 10 g L^{-1} were adjusted to pH 3 and 6 by addition of 0.01, 0.1, and 1 M HCl or NaOH, respectively. The solutions were sonicated with tip probe for 30 s (dispersive energy: 2.83 J L^{-1}; Labsonic M, Sartorius Stedim Biotech, Göttingen, Germany). Solutions of 0.005, 0.01, 0.05, 0.1, 0.25, 0.5, 1, 5, and 10 g TA L^{-1} were prepared and the pH values checked again. Electrolyte effects were tested at 0.02 M NaCl and 0.1 M $CaCl_2$ at pH 6 for TA concentrations of 0.01, 0.1, and 1 g L^{-1}. Additionally, 5×10^{-4} M $AlCl_3$ was added at a solution with 3 g TA L^{-1} until the pH reached 5, which partially induced the formation of Al–TA coprecipitates [30]. Before use, all initial solutions were sonicated again as described above. To test for colloidal properties of the TA, the TA solutions were analyzed for D_h and the zeta potential 24 h after ultrasonic treatment.

2.2. Freezing and thawing cycles

Freezing and thawing experiments were performed with 10 mL TA solutions filled in polyethylene tubes (volume 14 mL; inner diameter 14 mm). Separate tubes were prepared for DLS and CLSM measurements. Solutions used for DLS were reused in the consecutive FTC to keep the number of tubes manageable. In total, four tubes per TA solution corresponding to 1, 5, 10, and 20 FTC were used for CLSM measurements, and a fifth tube was stored at 4 °C as a reference. For freezing, the tubes were packed in a rack (distance between tubes: 0.5 cm) and placed in a styrofoam box (40 × 25 × 30 cm; wall thickness 5 cm) to delay freezing as under natural conditions. When transferred to the freezing chamber set to −20 °C, the temperature within the box reached 0 °C after 90 min (AFig. 2). Tubes were stored at −20 °C overnight and subsequently freeze-dried for CLSM measurements.

The effect of the size of the freezing cross-section on ice crystal growth and particle formation was tested using polyethylene tubes with 10, 14, 27, and 38 mm inner diameter, filled with 5, 10, 30, and 100 mL of TA solution, respectively. Samples in tubes with cross sections of 27 and 38 mm were first thawed at 20 °C in the laboratory atmosphere until the ice floated freely and finally in a water bath (15 °C $\leq$ T $\leq$ 20 °C), taking in total 4 h to reach 20 °C.

Tannic acid solutions with electrolyte addition were tested in tubes with 14 mm inner diameter in up to 10 consecutive FTC. For thawing, samples were stored in racks at room temperature, where tubes reached 20 °C, the temperature required for DLS measurements, within 90 min.

2.3. Particle sizing using dynamic light scattering

The D_h of TA particles in solution was analyzed by DLS (Zeta Pals, Brookhaven Instruments Holtsville, NY, USA) at a wavelength of 658 nm and a scattering angle of 90°. The measuring range is from 0.0001 to 1 % (vol./vol.) and the size range from < 1 nm to 6 μm. Directly after terminating the FTC by reaching 20 °C, solutions were transferred into a beaker and 3.5 mL were transferred with a pipette into a standard acryl cuvette. The D_h was recorded every minute for 5 min. Thereafter, the solution in the cuvette was transferred back into the beaker with the remaining TA solution, gently shaken, and the measurement repeated twice. Zero values and those above the detection limit of 6 μm were excluded. Up to 15 D_h values were obtained for each sample and used for calculating the median D_h.

2.4. Sizing and shape determination by confocal laser scanning microscopy

Tubes with frozen TA solutions were sealed with a 20-μm polyester mesh and freeze-dried. Upon loss of the ice matrix, TA particles concentrated mostly at the bottom of the tube. They were gently picked up with a brush and sprinkled on a glass slide to obtain even particle arrangements. The CLSM images were taken with a VK-9700 Violet Laser Colour 3D Laser Scanning Microscope (Keyence, Ōsaka, Japan) with a z-step size of 0.2 μm at 50 × magnification, resulting in an image size of 282 × 211 μm. The lower detection limit of particles was set to 0.1 μm^2 (equivalent to an ECD value of 0.3 μm). The ECD was used as size parameter most closely related to the D_h from DLS measurements in solution, being maximally 800 μm for the studied TA particles. Measurement areas were randomly chosen for samples containing small particles. In presence of large particles areas, we selected areas where particles were entirely imaged and not overlapping. Particles too large for visualization in one image were recorded in several images, which then were assembled. To determine the effect of TA concentration and number of FTC at pH 6 on ECD, in total 8,616 particles were analyzed, whereby 1,357 particles were evaluated for the sample with 0.01 g TA L^{-1} comprising relatively small particles and 83 for the sample with 10 g TA L^{-1} with relatively large particles (ATable 2). The particle shape was analyzed by elevation measurement using CLSM and evaluated with RStudio 1.3.1093 (RStudio, Boston, USA). Particles' greatest length (X_{max}), greatest length perpendicular to X_{max} (X_{mid}), and the greatest length perpendicular to X_{max} and X_{mid} (X_{min}) were used for determination of shape classes according to [31]. The subdivision of particles into seven different classes K, A, B, C_1, C_2, D_1 and D_2 is based on the ratios X_{max}/X_{min} and X_{mid}/X_{min} describing their spatial expansion (Fig. 2; ATable 1). To obtain a further subdivision within the range of very flat particles two additional classes (E_1, E_2) were defined. Mean elevations obtained by CLSM were used as estimate of particle height. Voluminous intricate structures of TA particles were additionally imaged after sputtering with gold by SEM (Quanta 200, Fei, Hillsboro, USA) at 15 kV using a secondary electron detector.

3. Results

During freezing of TA solutions, ice crystals grew inwards from the tube walls forming a brownish ice column in the tube center irrespective the background electrolyte used (AFig. 3a). At the bottom of the tubes, where ice crystals grew upwards, the column was more intensely colored and had entrapped air bubbles. Upon freeze-drying, the brownish column in the center of the tubes remained at TA concentrations of 5 and 10 g L^{-1}, indicating a pronounced connectivity and stability between TA particles formed (AFig. 3b). In contrast, at TA concentrations $\leq$ 1 g L^{-1}, TA particles accumulated only at the bottom of the tubes.

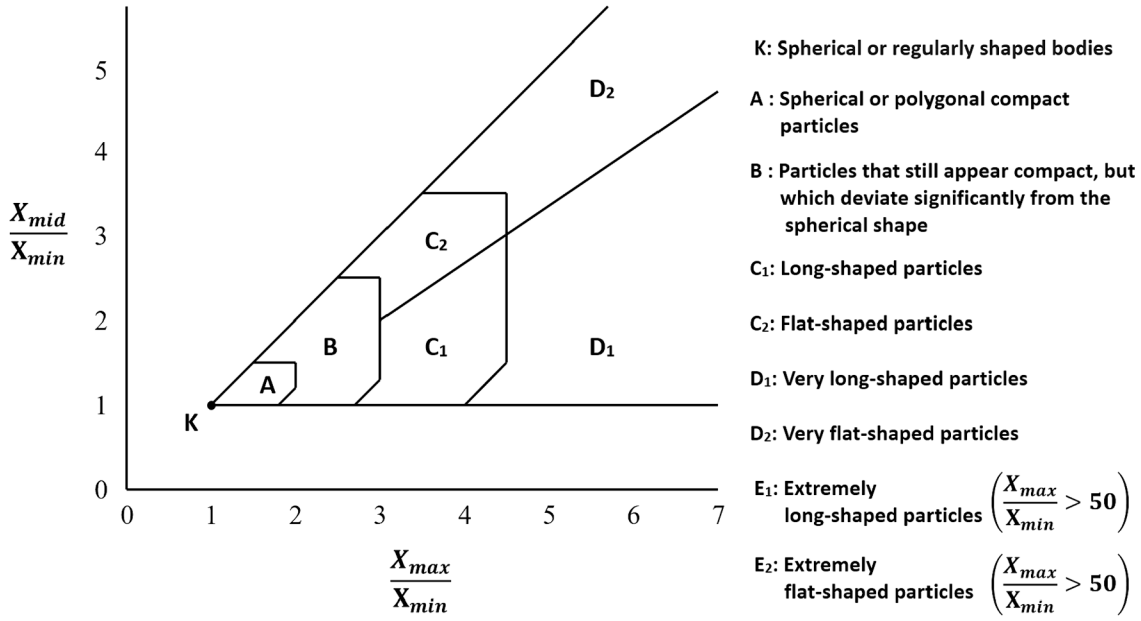

Fig. 2. Modified classification diagram for particle shapes. For classes E_1 and E_2 only boundary conditions are reported. adapted from [31]

3.1. Micromorphology of tannic acid particles

Both, the concentration and number of FTC influenced the size and morphology of formed TA particles as revealed by CLSM at uniform magnification (Fig. 3a–h). Upon single freezing of 0.01 g TA L^{-1} solution at pH 6 and without electrolyte addition, most of the particles were very small, with needle-like shape (Fig. 3a). With increasing TA concentration, the size of particles increased, with increased shares of platy particles (Fig. 3e). For a given TA concentration, the size of particles increased with increasing number of FTC (AFig. 4a–h), and for 0.01 and 0.1 g TA L^{-1} and 20 FTC, the large particles forming featured marked surface roughness (Fig. 3d, h). In contrast, particles formed at 1 and 10 g TA L^{-1} showed flatter shapes and smoother surfaces (AFig. 4e–h, AFig. 5a–f). Circular holes in platy particles were preferentially observed at low and high TA concentrations, respectively (Fig. 3g, AFig. 4 g).

The varying morphologies of TA particles formed at pH 6 upon different number of FTC indicates various modes of formation. For 1 g TA L^{-1} after 5 FTC, a fibrous network of flat-shaped platy particles formed, where typically three fibers created a connection and the space between the fibers was filled by a thin layer (AFig. 6a). Fractured surfaces at the edges might have been due to tension cracks and movement of the brittle samples. In addition, holes appeared in platy particles, with bulging outer rings at the rim of the holes as well as at particle edges (AFig. 4b). After 10 FTC, thick, compact particles with pronounced surface roughness were formed (AFig. 6c). Increasing freezing cross-sections resembled particle micromorphologies obtained in the experiments with different TA concentrations at an inner diameter of 14 mm (AFig. 7a–d; Fig. 3).

Electrolyte effects on the morphology of freeze-dried TA samples could only be studied for the NaCl and $AlCl_3$ additions since TA particles formed in presence of $CaCl_2$ were very hygroscopic in contact with air and immediately formed large secondary aggregates after freeze-drying. Particles that formed at 0.1 g TA L^{-1} in presence of NaCl at pH 6 after 5 FTC were compact and had frizzy grained surface morphologies, with partial encrustation and fractures (AFig. 6d). The addition of $AlCl_3$ had a similar effect on the morphology of TA particles as the NaCl addition (AFig. 8).

In addition, scanning electron microscopy analysis of voluminous particles formed at low to high TA concentrations at pH 6 after 5 and 20

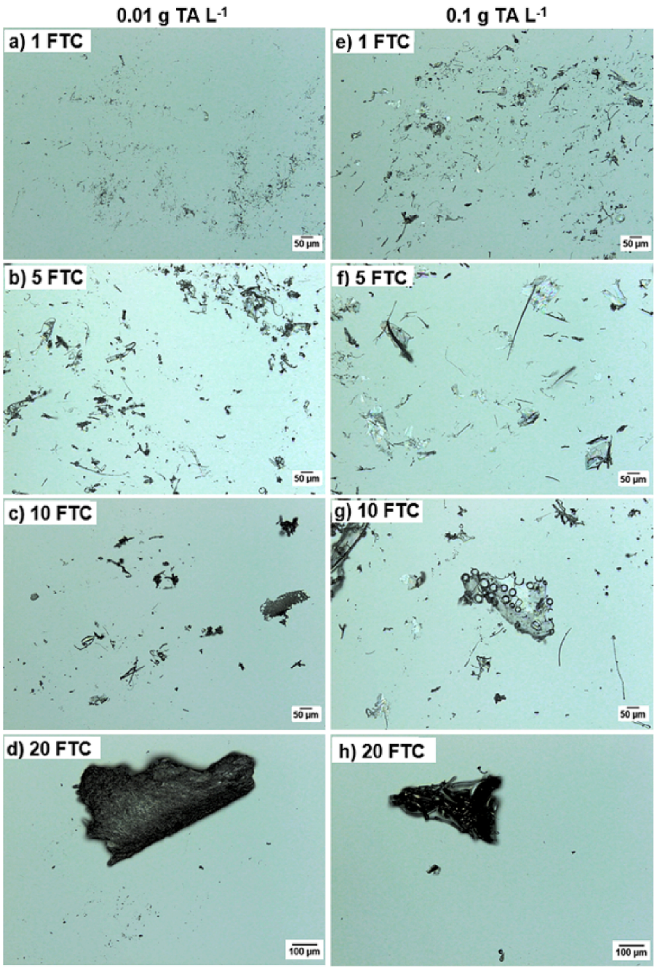

Fig. 3. Confocal laser scanning microscopy images of TA particles formed at pH 6 and without electrolyte solution for 0.01 and 0.1 g TA L^{-1} and at 1, 5, 10, and 20 FTC. Magnification: 10×.

FTC, respectively, showed net-like structures, mainly consisting of fibers and plates (Fig. 4a–d). The fibers were thicker than the plates and usually three to four fibers were interconnected. Connected fibrous structures, with fibers being either curved or straight, were found for particles formed at 0.1 g TA L^{-1} (Fig. 4a,b). These fibers likely formed at three-grain boundaries. Fibers were partly interlinked by thin plates (Fig. 4b). Particles formed at TA concentration of 10 g L^{-1} were less fibrous, with net-like structures, comprising thin plates and cavity spaces between the fibers, indicating formation at two-grain boundaries (Fig. 4c,d). For fibers connected at an angle of ~ 120°, a fourth fiber could emerge from the conjunction perpendicularly, resulting in a 3D net structure (detail image in Fig. 4b). In SEM images of TA particles formed from solutions with $AlCl_3$ additions, platy particle shapes dominated (**AFig. 9**).

3.2. Size of tannic acid particles depending on experimental conditions

3.2.1. Effect of tannic acid concentration and number of freeze–thaw cycles at pH 6 and 3

Freeze-thaw cycles conducted at pH 6 and 3 without addition of electrolytes resulted in a wide spectrum of TA particle sizes with ECD values ranging from 0.3 to > 50 μm (Fig. 5). Irrespective of the TA concentration and the number of FTC, ECD of particles formed at pH 3 were generally larger than those formed at pH 6, i.e. small particles (ECD < 1 μm) were far more abundant at pH 6 than at pH 3. While increasing numbers of FTC led to an increase in the share of particles > 10 μm at pH 6, a moderate opposite trend was observed at pH 3. Here, the share of large particles decreased in favor of medium-sized (1–10 μm) ones (Fig. 5, **ATable 2**). Overall, for both pH higher TA concentrations resulted in larger ECD values, particularly increasing the share of particles > 10 μm.

The D_h of the original TA solutions at pH 6 and 3 without freezing indicated a concentration effect, with a trend towards higher D_h at low TA concentrations (Fig. 6). The principal trend of higher numbers of FTC resulting in the formation of larger TA particles observed for pH 6 held true also for pH 3. This was most striking at low TA concentrations (≤ 1 g L^{-1}), whereas for 5 and 10 g TA L^{-1} the D_h remained close to the reference solution without freezing. However, maximum D_h values at pH 3 were markedly lower (2.60 ± 1.24 μm) than those at pH 6 (3.65 ± 1.11 μm).

After 5 and 10 FTC, the scattering signal was lost for all studied TA concentrations but returned upon releasing particles from the tube walls using a laboratory rubber wiper. Some particles likely disintegrated upon wiping as the measured D_h values were partly smaller than those observed before. However, D_h values observed towards higher numbers of FTC were again larger, indicating that in the experiment with consecutive freeze–thaw events, the particle sizes were mostly restored after wiping.

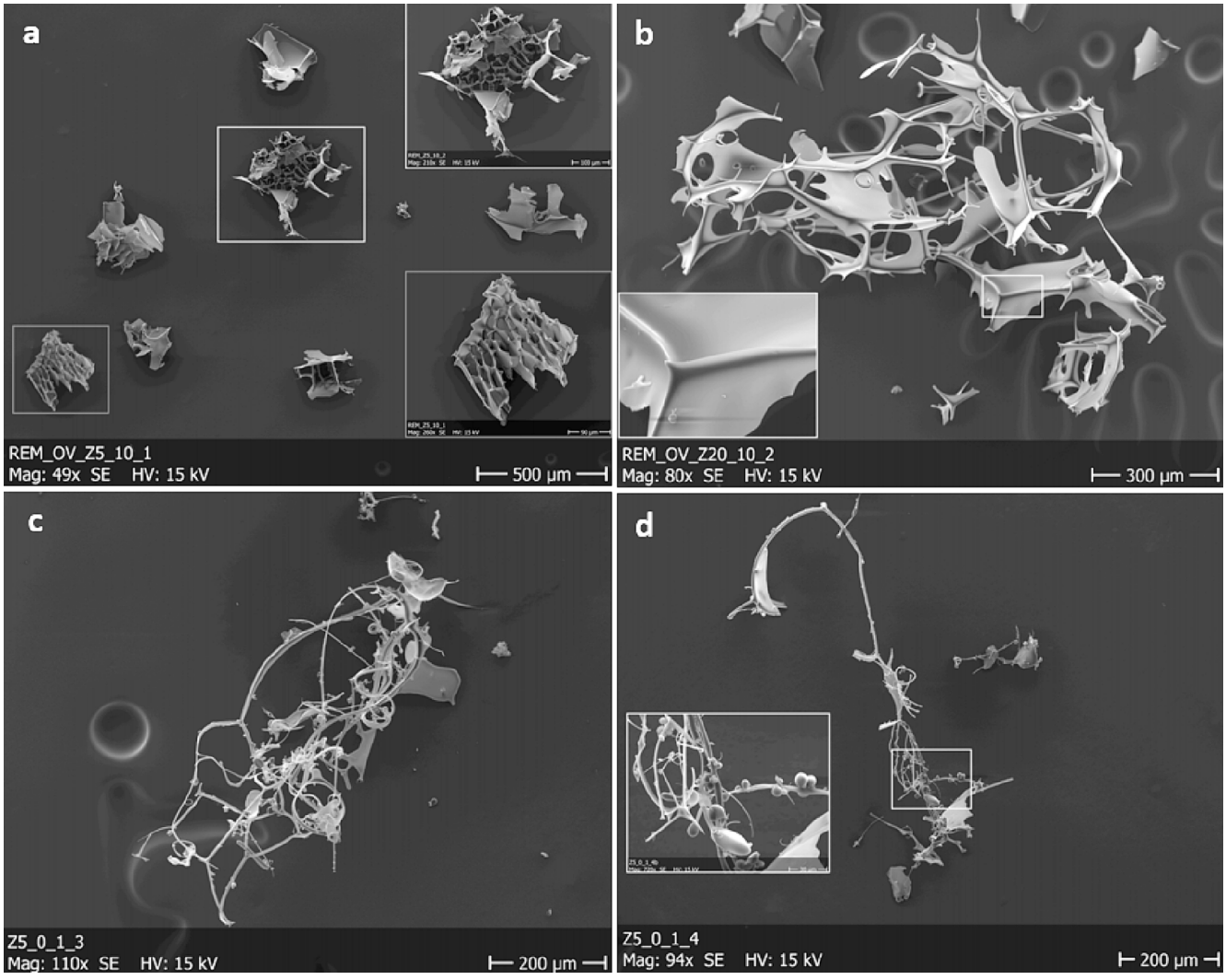

Fig. 4. Scanning electron microscopy images of TA particles formed at pH 6: (a, b) 0.1 g TA L^{-1} and 5 FTC. (c) 10 g TA L^{-1} and 5 FTC. (d) 10 g TA L^{-1} and 20 FTC.

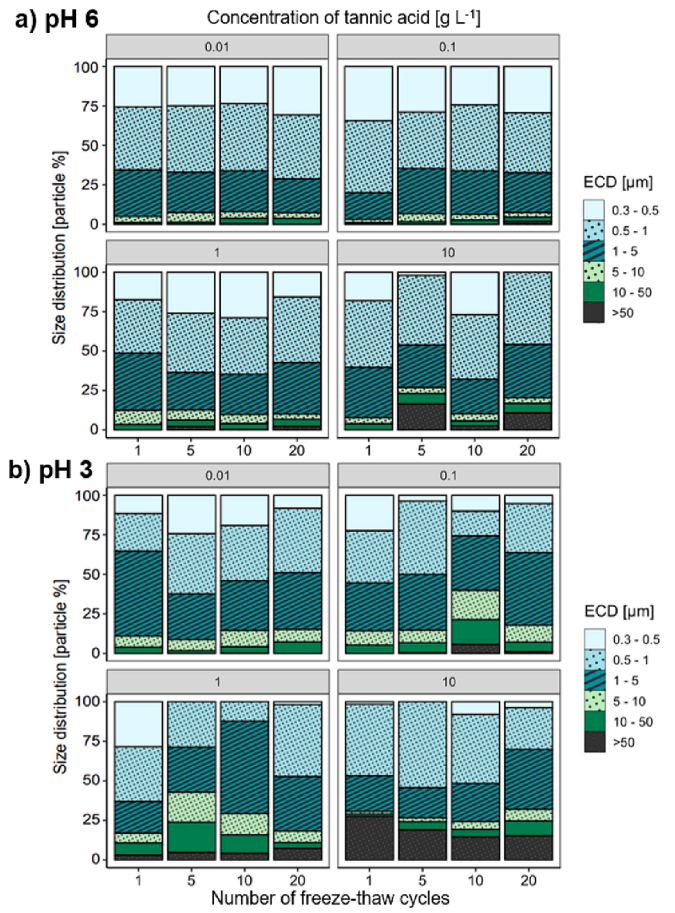

Fig. 5. Equivalent circle diameter (ECD) of TA particles at (a) pH 6 and (b) at pH 3 as depending on TA concentration and number of FTC. For data evaluation, 83–1357 and 42–585 particles were considered, respectively (ATable 2).

3.2.2. *Influence of freezing cross-section (pH 6)*

For the FTC conducted at freezing cross-sections of 10, 14, 27, and 38 mm, the mean ECD of particles increased towards higher TA concentrations within one tube size by factors 4, 2, 18, and 3 (AFig. 10; ATable 5). With the increase in tube diameter from 10 to 38 mmm, the ECD of particles formed after the first freezing event increased for 0.01 g TA L^{-1} by factor 3, for 0.1 g TA L^{-1} by factor 2, and for 1 g TA L^{-1} by factor 1.3. Thus, higher TA concentration and larger freezing cross-section resulted in higher ECD after the first freezing (AFig. 10). The effects of consecutive FTC on ECD values depended on the situation after the first freezing: If large particles formed, consecutive FTC had rather a destructive effect and resulted in an increase in medium-sized particles mainly in the 1–5 µm range. However, if there were only few large particles, their proportion increased with the number of FTC. In sizing experiments with the thawing solutions, the D_h typically increased after one FTC for all studied TA concentrations and all freezing cross sections (AFig. 11; ATable 6). Overall, there was no clear effect of the size of freezing cross sections on the D_h values of suspended TA particles.

3.2.3. *Electrolyte effects (pH 6)*

The positive influence of increasing numbers of FTC on the formation of large particles > 10 µm was evident for both $AlCl_3$ and NaCl systems (AFig. 12), but most pronounced when compared with experiments without electrolyte addition (Fig. 5). For high numbers of FTC, NaCl addition caused higher percentages of particles with ECD > 50 µm than the addition of $AlCl_3$. For 0.01 g TA L^{-1}, the > 50 µm fraction increased from 0 to 21 % during 5 FTC. The share of large particles for 1 g TA L^{-1} with NaCl added was already high after the first freezing event (19 % particles > 10 µm), and increased after 10 FTC (56 % particles > 10 µm).

In the thawed state, addition of NaCl to solutions of 0.01−1 g TA L^{-1} did not markedly change the D_h values of the original TA solutions (Fig. 7; ATable 8). The D_h for 1 g TA L^{-1} changed little during the first freezing–thawing event but then increased steadily with more FTC (Fig. 7). Larger initial D_h values were measured in $CaCl_2$ and increased steadily with the number of FTC. The largest initial D_h of 5.74 µm was measured for 1 g TA L^{-1}, but decreased already strongly during the first 5 FTC (Fig. 7). Addition of $AlCl_3$ caused the smallest initial D_h values in unfrozen TA solutions of all three electrolytes tested. It needs to be considered that $AlCl_3$ addition to TA solution can partially induce the formation of Al–TA coprecipitates, which might affect D_h measurement. Overall, the results indicate that increasing number of FTC caused increasing D_h values for all TA concentrations, being highest for the 0.1 g TA L^{-1} and smallest for the 1 g TA L^{-1} solution (Fig. 7).

3.2.4. *Shape classes*

The morphological classification of TA particles formed at pH 6 and 3 revealed a general trend towards particles becoming flatter with increasing particle size (Fig. 8; AFig. 13). The influence of the number of FTC on particle shape was little for all TA concentrations. In the fraction > 50 µm, compact particles (A, B) disappeared with increasing number of FTC. More platy particles with diameter > height formed at larger ECD, while the amount of compact and needle-like particles decreased. At pH 6, the shape of particles with an ECD of 0.3−0.5 µm was compact (shape class A and B; 17−23 %) or long-shaped (shape class C_1-E_1; 77−84 %), independent from the number of FTC. At pH 3, this proportion of shape classes for 0.3−0.5 µm TA particles was observed after one single freezing event only (AFig. 13). Towards larger particle sizes, the share of compact particles diminished and elongated particles D_1 with a X_{max}/X_{min} ratio between 4.5 and 50 became more prominent. In the largest size fraction > 50 µm, flat particles generally dominated, with the highest share (77 %) after 20 FTC. The formation of extremely flat particles E_2 ($X_{max}/X_{min} \geq 50$) was observed in all size fractions > 0.5 µm (Fig. 8), reaching a maximum share of 25 % after 10 FTC.

For all freezing cross-sections, particles in the finest fraction 0.3−0.5 µm were compact (A and B) or elongated (C_1-E_1) (AFig. 14). After one freezing event, the percentage of compact particles with shape class A and B were 58, 20, 21, and 50 % for freezing cross sections of 10, 14, 27, and 38 mm, respectively. The share of compact particles decreased with increasing particle size and increasing number of FTC as well as for all freezing cross-sections. This holds true for inner tube diameters of 10 and 14 mm for all size fractions, while for those > 14 mm a decrease in compact particles occurred for size fractions < 10 µm.

Addition of NaCl generally promoted the formation of compact shapes, while the proportions of elongated and very flat shapes were lower than with $AlCl_3$ or without additive (AFig. 15). $AlCl_3$ as background solute produced compact particles in the size fraction < 0.5 µm (62 % of classes A and B) after one freezing event, but the contribution of compact particles decreased towards coarser sizes, being even absent in the largest size fraction > 50 µm. Platy particles (C_2-E_2) were present in all size fractions > 0.5 µm after one freezing event, reaching a maximum contribution of 86 % in the > 50 µm fraction (AFig. 15). With increasing number of FTC, the particle shape pattern basically didn't change, though there was an increase of very flat particles (E_2) after 10 FTC. For the NaCl addition, the portion of compact particles < 0.5 µm (A and B) was 12 % after one freezing event, and thus much lower than for the $AlCl_3$ treatment or TA without electrolyte addition (Fig. 8, AFigs. 14 and 15). However, the share of compact particles was higher in all other larger size classes, exceeding even the respective proportions of the $AlCl_3$ treatment (AFig. 15).

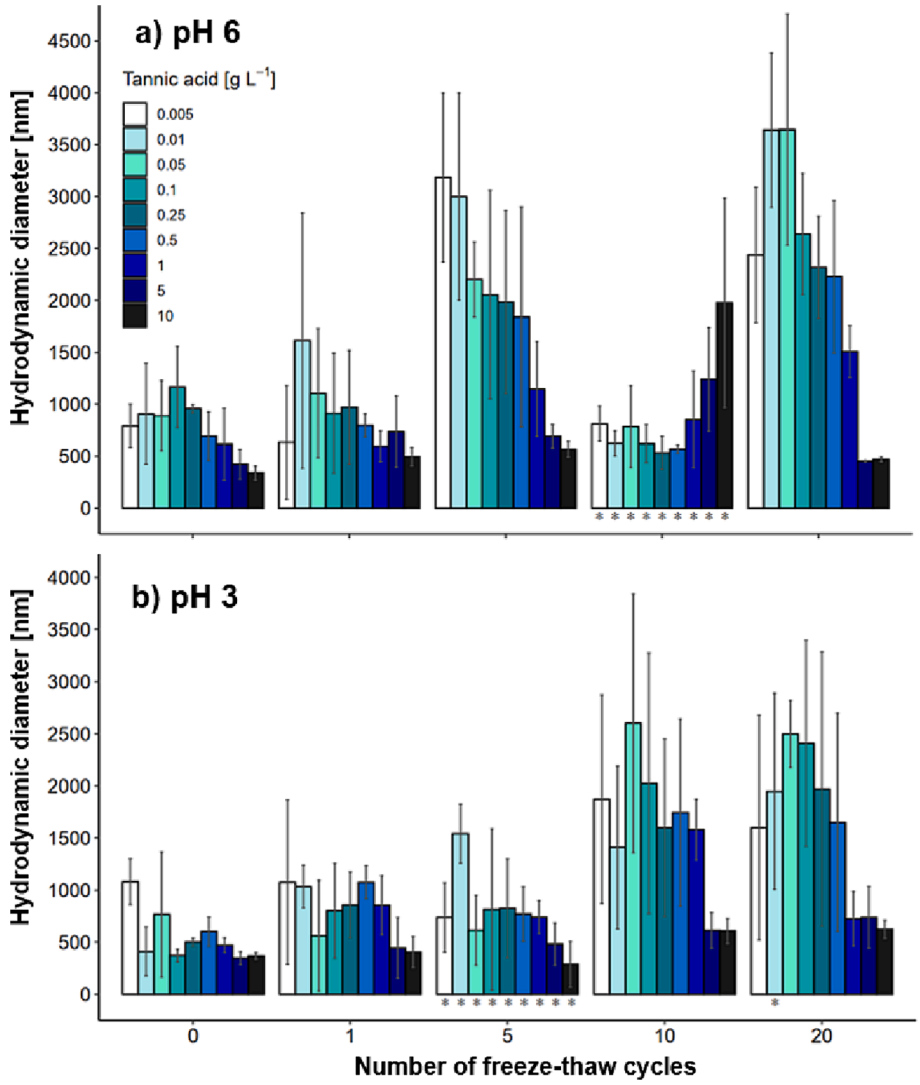

Fig. 6. Hydrodynamic diameter of TA particles at (a) pH 6 and (b) at pH 3 as depending on TA concentration and number of FTC. For samples marked with asterisks, TA particles attached to the walls of the tube were transferred back to solution with a laboratory rubber wiper. The number of runs for samples and the error of the method is given in **ATable 3 and 4**.

4. Discussion

4.1. Particle formation by freezing

The ECD of TA particles showed a wide size range from 0.44 to > 300 μm, with most particles being < 5 μm. It is known that the presence of solutes and colloids can restrict the growth of ice crystals drastically, resulting in smaller ice particles [32,33]. Hence, an increasing TA concentration should increase the number of ice crystal boundaries, and thus, the volumes, with solutes becoming trapped and remaining unavailable for further freeze-concentration (Fig. 9f). In result, smaller TA particles are formed due to more ice crystal boundaries.

While the grain size of ice crystals was not directly determined in our experiments, it can be deduced from the dimensions of the particles formed, i.e., the shapes derived from microscopy (Figs. 3 and 4, **AFig. 6**) and the ECD sizes obtained by CLSM (Fig. 5, **AFigs. 10 and 12**). Both imaging techniques applied, CLSM and SEM indicate that sub-grain boundaries of ice crystals formed mostly idiomorphic as TA molecules are variable in shape and can undergo marked loss of volume upon freezing (Figs. 3 and 4, **AFig. 6**). The observed ECD values of TA particles (up to 700 μm) was in the range of average ice crystal sizes observed for different suspensions with particles of soda glass, alumina, and silica [15,32].

Largest particles with ECD ≥ 10 μm were found for concentrations ≥ 1 g TA L^{-1} (Fig. 5; **ATable 3 and 4**), emphasizing the role of freeze-concentration. Principally, exclusion and entrapment of impurities is controlled by the velocity of the solidification front, depending on various factors such as size of impurities and viscosity (Fig. 9a–f). Low temperatures can cause higher viscosity, reducing the mobility of particles, which hinders the segregation process to form pure ice. In case ice crystallization is restricted by rapid freezing or high viscosity, segregation is limited and the concentration of solutes in the liquid will be less than the theoretical eutectic mixing ratio [34]. Where planar ice growth changes to lamellar ice growth, freeze-concentration is a self-limiting process [12], (Fig. 9b and e).

4.2. Particle formation traced by hydrodynamic diameter

In the original solutions prior to freezing, the D_h values of TA were in a broad range from 350 to 1,170 nm, independent of pH and with lowest values for the highest TA concentration (Fig. 6), suggesting that TA was present in a stable self-aggregated state [30,37]. At both studied pH values, 3 and 6, an increasing number of FTC increased the D_h of TA particles, especially at low TA concentrations. This is best explained by

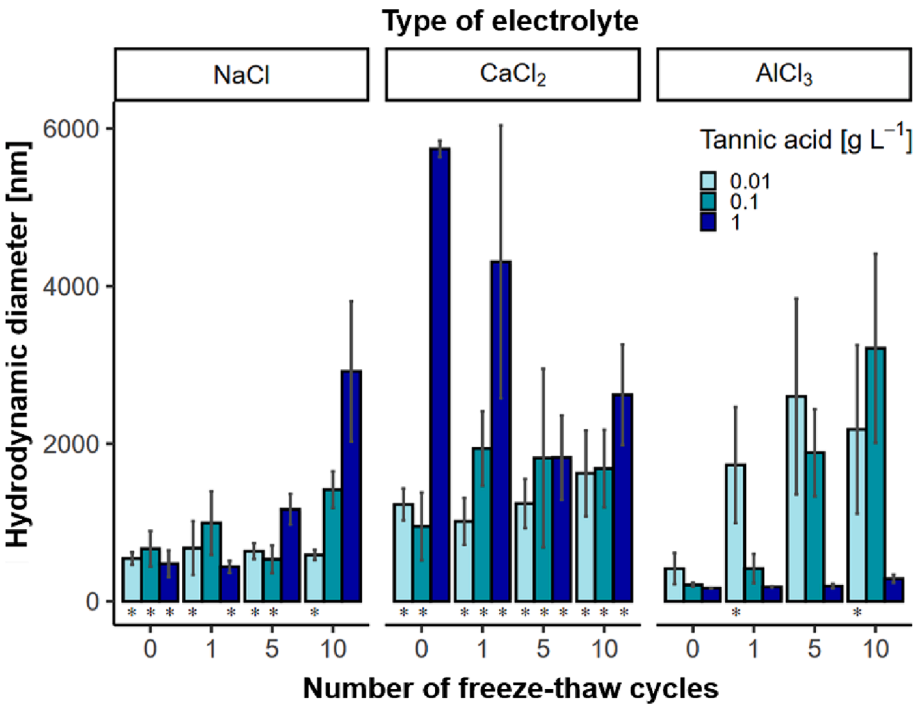

Fig. 7. Hydrodynamic diameter of TA particles depending on TA concentration, number of FTC, and presence of different electrolytes. The number of runs per sample and the error of the method is given in ATable 8.

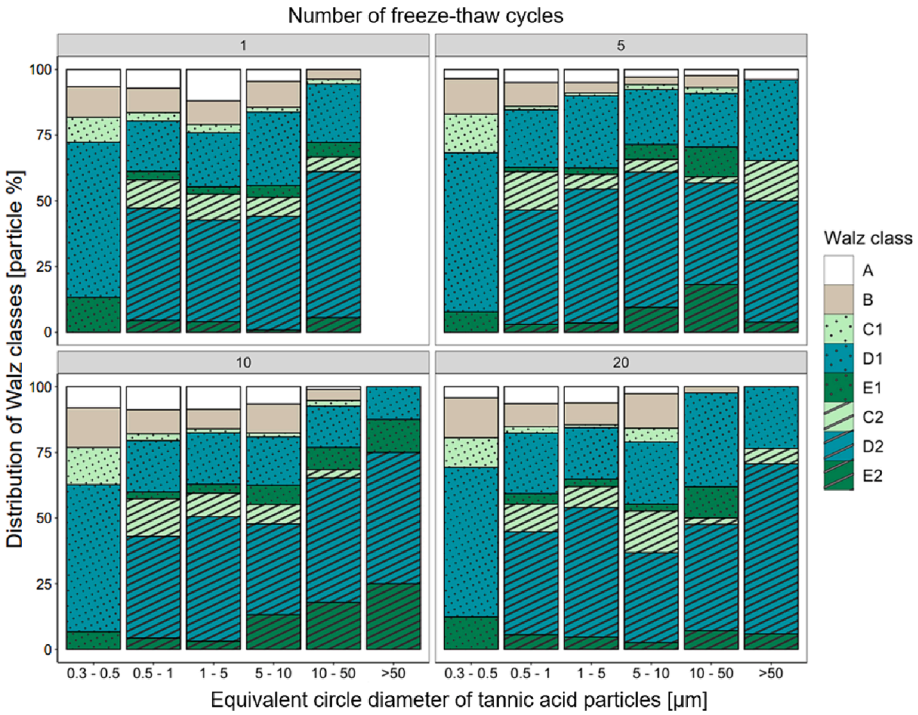

Fig. 8. Distribution of the TA particles over shape classes according to [31], depending on particle size and the number of FTC at pH 6, averaged over all concentrations. Definition of shape classes is given in Fig. 2.

two mechanisms during ice crystal growth, the separation of accumulation zones and the aggregation of particles in a decreasing volume (Fig. 1, Fig. 9e), [12]. Aggregation of initially large TA particles facilitates the formation of even bigger particles, aside from the occurrence of a high number of small particles. This is because large particles diffuse slower than small particles, resulting in smaller particle–particle distances and enhanced aggregation during freezing.

The D_h of TA solutions adjusted to pH 3 and 6 remained almost constant after one single freezing and thawing event (Fig. 6). A considerable enlargement of the D_h occurred between 5 and 10 FTC, while more cycles caused only little changes. This trend can be explained by the fact that initial freezing removes TA from solution. Lower TA concentrations resulted in the formation of larger ice crystals and stronger crystallization pressures during later freezing events and was

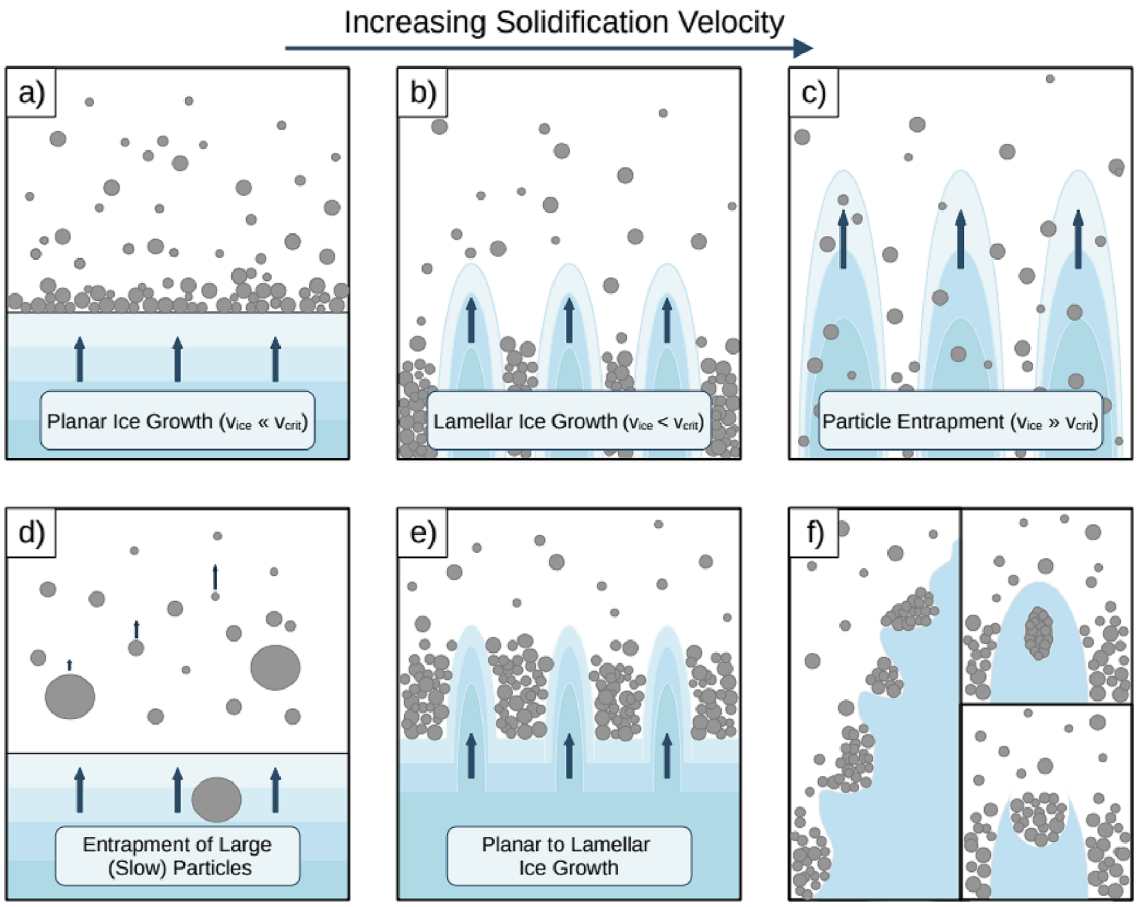

Fig. 9. Simplified freezing mechanisms for solid particles smaller than ice crystals. The critical velocity controls the rejection and entrapment of particles, which defines the highest velocity of solidification where particles can escape by diffusion. For slow solidification, ice-growth is planar (a). With increasing velocity, the ice has to squeeze between the particles, resulting in lamellar or cellular structures (b). When particles have insufficient time for segregation, they will be entrapped by the ice (c). Larger and slower particles are first engulfed ($V_{crit} \propto 1/radius$) (d). With increasing concentration, diffusion of particles is restricted, and ice grows in lamellar structures (e). The surface of growing ice possesses cavities where particles can be trapped as well (f). Summarized in modified form from [12,35,36].

likely responsible for the increase in D_h between 5 and 10 FTC. Obviously, this effect applied also to the low concentrated TA solutions, where large TA particles were formed in the first FTC. With increasing FTC, a trend for increasing D_h values was observed, which was not always uniform (Fig. 6). Likely, the more unstable particles became dispersed upon thawing. With increasing number of FTC, however, reassembling of smaller units caused increasing particle sizes. The non-uniform increase and the high median of D_h values suggest a polydisperse particle size distribution, with the range of particle sizes present in solution increasing with the number of FTC (Fig. 5, **AFigs. 10 and 12**). For soil aggregates, it has been shown that changes in the size occur until the majority of particles reached their specific stable size under given cryogenic conditions [5]. This implies that particles above the specific size did not outlast the thawing process and partly become dispersed. Hence, the evaluation of the D_h values indicated that freeze-concentration enhances particle aggregation but can induce dispersion as well.

4.3. Effects of tannic acid concentration on particle size

We hypothesized (i) that TA concentration affects the size of ice crystals with larger crystals and TA particles forming at low concentration. Based on the formation of relatively large particles at low TA concentrations upon freezing as observed by CLSM, the formation of larger ice crystals is obvious (Fig. 5). Higher TA concentrations cause thicker sub-grain boundaries, since the maximum accumulation of TA in a certain volume is limited by the eutectic concentration.

According to CLSM and SEM, large particles occurred in frozen state and partly persisted after thawing, with largest D_hs being found for the lowest TA concentrations (Fig. 6). An explanation for the formation and preservation of large particles from initially low concentrated TA solutions can be a higher crystallization pressure of ice combined with localized heat production [38,39], enhancing the aggregation and stability of particles. However, D_h values increased upon FTC for all TA concentrations. The increases of up 6.5 times were found for concentrations ≤ 0.1 g TA L^{-1} and up to 1.7 times for ≥ 5 g TA L^{-1} (Fig. 6). The results from both methodological approaches in the thawed (D_h) and dry state (ECD) support hypothesis (ii) that FTC result in amplification of self-aggregation.

4.4. Impact of freezing cross-section

Freeze-concentration of non-aqueous constituents should be theoretically stronger if the ice front spreads over a longer distance (hypothesis (iii)). Evaluation of the ECD by CLSM in the dry state revealed that particle sizes increased with increasing freezing cross-section. In addition to the spreading distance of ice crystals, it has to be considered that the volume of the freeze-concentrated solution increases with the initial TA concentration and for the same concentration with total mass of solute affected by freeze-concentration, which increases with the inner diameter of the tube. Since the freeze-concentration stops at the eutectic mixing ratio, the volume of concentrated solute was larger for a more available solute mass at high cross sections (**AFig. 16**). Thus, the percentage of large particles (≥ 10 μm) increased with freezing cross-

section for a given concentration. Likely, the occurrence of large particles can rather be explained by the higher supply of TA with increasing cross-section than by the spreading distance of ice crystals.

4.5. Influence of pH on tannic acid particle size

We assumed that at low pH, where repulsive forces between TA molecules are decreased, self-aggregation upon freeze-concentration is amplified and formation of larger particles favored (hypothesis (iv)). When investigating the effect of FTC on D_h values at pH 3 and 6, however, we observed slightly higher D_h values at pH 6 (Fig. 6), contradicting our expectation. As the D_h used for sizing is prone to modifications in solution by dispersion (section 4.2.), evaluation of ECD results appears more reliable. They indicated larger particles for all TA concentrations and enhanced aggregation at pH 3 compared to pH 6 (Fig. 5). The increasing TA aggregation at lower pH needs also to consider pH changes during freezing, as protons are increasingly concentrated in the remaining liquid. At pH values < 3, the D_h of TA increased [30], which was explained by a reduction of the net negative charge of TA. This allows TA molecules to overcome the repulsive barrier by their Brownian motion and to form aggregates, involving both hydrogen bondings [40] and hydrophobic interactions [41]. The effect was observed in frozen state only and did not persist in the thawed state as the initially rejected and finally trapped solutes are back-released into solution upon thawing, resulting in a re-shift of the pH. A similar observation has been reported for proteins for various buffers, where the effect of pH on aggregation was less than that of the freezing rate [42]. Concentrations of ions from NaOH and HCl additions for pH adjustment are affected by ice growth, too. Although rejection of large molecules during ice growth is 1.4 to 1.7 times higher than for inorganic ions (Fig. 9), strong shifts of pH in the remaining liquid have been observed for freezing systems [19,34]. For TA solutions adjusted to pH 3, this would result in a shift to even more acidic conditions, theoretically further promoting aggregation.

4.6. Electrolyte effects on tannic acid particle formation

As TA is prone to metal complexation, we studied the effect of mono- and multivalent cations on the self-aggregation and stability of TA particles during freeze–thaw cycles (hypothesis (v)). The ECD of TA particles formed by freezing in presence of NaCl and $AlCl_3$ increased with increasing number of FTC (**AFig. 12**). Samples with $CaCl_2$ addition remained moist, as the eutectic mixture of $CaCl_2$ has a freezing point of $-50.4\,^{\circ}C$ ($-21.3\,^{\circ}C$ for NaCl), [43], making sublimation of water during freeze-drying incomplete. In presence of NaCl and $AlCl_3$, the percentage of large particles $> 10\,\mu m$ was higher than without electrolyte additions. Contrary to the expectation based on the valency of the cations (hypothesis (v)), largest ECD were obtained for NaCl. The reason for this observation likely is that the solute mass was higher for NaCl than for $AlCl_3$ (20 mM versus 1.7−170 μM). As the negatively charged ice surfaces at pH > 4 [44] provide additional adsorption sites for cations, the actual number of cations being able to promote TA aggregation via charge screening might have been much lower for the $AlCl_3$ than NaCl treatment, because Al becomes more strongly bound to the ice. This counteracts the potential ability of Al to induce TA aggregation by forming bridges between TA molecules. For the thawing solutions, the comparison of the D_h with electrolyte additions indicates a higher particle stability with higher cation valency.

4.7. Shape classes

Confocal laser scanning microscopy revealed spherical-compact, elongated, and flat shapes of TA particles, with the latter two being most common (Fig. 8). Occasionally, 3D net structures comprising both particle shapes were observed (Fig. 4). These filigree structures are remnants from the central column formed within tubes and most of them collapsed upon removing the supporting ice matrix. The shape of these particles was interpreted under the assumption that disintegration occurred uniformly for all samples, allowing for the description of relative differences. For compact particles it is likely that these represent the shape of TA aggregates in solution, which remain intact if entrapped by the advancing ice front. The omnidirectional crystallization pressure of the ice growing around the particles should have favored compact shapes, whereas particles in the diminishing liquid volume underwent compression and shaping by growing ice crystal faces. Elongated and flat shapes are products of freeze-concentration, with the former type corresponding to three-grain boundaries and the latter to two-grain boundaries (Fig. 1). Since three-grain boundaries are energetically more favorable for solutes [45], it is plausible that fibers are formed preferentially at lower TA concentrations. Size and shape thus corresponded to the form and volume of the sub-grain boundaries of the ice.

Additions of $AlCl_3$ and NaCl induced preferential formation of large particles with ECD $\geq 10\,\mu m$, and their share increased with the number of FTC for all concentrations. At 1 g TA L^{-1} and 10 FTC, particles with an ECD of 10−50 μm predominated for $AlCl_3$ addition, while for NaCl the particles $> 50\,\mu m$ dominated. Together with the occurrence of large particles, the number of compact particles increased, most pronounced for NaCl addition especially after 5 FTC. Obviously, large TA aggregates formed in presence of NaCl, where their size supported engulfment in the ice (Fig. 9d).

4.8. Comparison of methods for particle characterization

Sizing of TA particles formed in FTC was performed by DLS in the thawed state and by CLSM after freeze-drying. Particle sizes analyzed by both methods suggest a contrary effect of the TA concentration. In the thawed state, DLS showed that the largest particles sizes were related to the lowest TA concentration and *vice versa*. In the dry state, CLSM revealed the largest particles size for the highest TA concentrations. Supported by determinations of particle shape, the findings could be well-assigned to different mechanisms: More filled sub-grain boundaries of ice crystals at high TA concentrations result in large platy particles. Low material supply to fill the sub-grain boundaries at low TA concentrations results in smaller, elongated particles only forming at three-grain boundaries. Though large particle sizes existed in the dry state after freezing at high concentrations, they dispersed upon thawing. In contrast, TA particles formed at low concentrations were exposed to a higher crystallization pressure of larger ice crystal faces [38] and therefore seem more resistant against dispersion. Thus, increased stability and decreased dispersibility can be another reason for the observation of relatively high D_h values at low TA concentrations. The effect increased with the number of FTC, although an upper limit of enlargement is likely. For freezing of clay mineral suspensions, stable aggregation outlasted into the thawed state [46], indicating that aggregates formed from clay minerals are likely to have a higher stability than the aggregates of TA studied in our experiments. Overall, the results obtained by both methodological approaches are not directly comparable but complement each other by providing information on particle forming by freezing and thawing.

4.9. Possible applicability to natural conditions

As TA or other high-molecular weight organic molecules, DOM features amphiphilic properties, which my result in similar (self-)aggregation as observed for our model TA system. For example, in simulations of the structure of aggregated organic colloids, lipid tails and other hydrophobic fragments form the core, while hydrophilic functional groups are exposed to water, where cations can connect the molecular moieties [47]. We assume that results obtained for freezing-thawing and particle formation in TA solutions can also be transferred to organic colloids in aquatic systems and soils, where size and shape of particles formed play a decisive role for their function [19,48,49].

Despite freezing of TA solutions was induced by a large temperature gradient, freeze-concentration took clearly place, indicating that the velocity of the solidification front was always below the critical velocity, resulting in planar ice growth (Fig. 9a). However, in soils, freezing can be much slower, depending on water content, pore size distribution, and factors governing the removal of heat of crystallization. A very low growth rate of ice crystals favors the exclusion of solutes and colloids and enhances freeze-concentration [12].

Unlike aquatic systems, soils consist of a solid matrix with pores variably filled with air and water. In general, freeze-concentration for a given organic solute or colloid concentration is more distinctive for larger pore volumes (**AFig. 16**). Freeze-concentration likely amplifies the formation of larger organic particles, resulting in a reduced microbial decomposition due to the lower external surface and reduced accessibility [50]. In permafrost soils, vertical migration and subsequent precipitation of organic solutes and colloids during ice segregation along freezing gradients, a process defined as "cryogenic retinization" [51], is considered as a major process in the formation of stable organic matter at the permafrost table [52].

At the other hand, zones of concentrated organic matter can enhance the local availability of substrates and nutrients, representing hotspots of microbial life in frozen environments. In Antarctic ice induced by freezing point depression, connected liquid veins with stocks of concentrated carbon exist along the grain boundaries, enabling survival of microbiota for decades [11,17].

5. Conclusions

In comparison with previous studies on freeze-concentration and particle formation considering dispersed colloids [5,12,32], we could show that organic particles formed from TA solutions most closely resemble the ideal morphology of the sub-grain boundaries of ice crystals. This is supported by the relatively slow velocity of ice solidification, favoring planar ice-growth and enabling TA molecules to escape from ice entrapment by diffusion. Moreover, TA molecules adjust closely to the shape of ice crystals in the residual volume, leading to various spatial properties of TA aggregates. The freeze-concentration effect was most intense at low TA concentrations and increased with the number of FTC. Largest particles were observed at pH 3 and in presence of electrolytes, which is due to changes in amphiphilic properties, conformation, and aggregation. Particle size characterization by D_h and ECD in the thawed and dry state after freezing, respectively, revealed a contrary impact of the TA concentration. In the thawed state, the largest particles sizes are related to the smallest TA concentration and *vice versa*, in the dry state the largest particles size were obtained for the largest TA concentrations. The preservation of large particles from initially low concentrated TA solutions indicates enhanced stability of particles, which is due to a higher crystallization pressure of ice [35]. Results obtained for particle formation by freezing of TA solutions may also apply to organic solutes and colloids in aquatic systems, where the structure and reactivity of organic particles and consequently their function is of high interest [48,49]. Freezing-induced formation of larger organic particles in soils could render them less biologically available. This may explain the enrichment of organic matter in permafrost soils at the permafrost surface [52]. In presence of reactive minerals, freeze-concentration could also foster the formation of mineral-organic composites [36]. However, whether this increases the stability of organic matter warrants further research as concentration of organics may also create microbial hotspots after thawing [53].

CRediT authorship contribution statement

Stefan Dultz: Conceptualization, Methodology, Writing – review & editing. **Myriam Speth:** Methodology, Investigation, Visualization, Data curation, Validation, Formal analysis, Writing – original draft. **Klaus Kaiser:** Writing – review & editing, Funding acquisition. **Robert Mikutta:** Writing – review & editing, Funding acquisition. **Georg Guggenberger:** Writing – review & editing, Funding acquisition, Supervision, Resources, Project administration.

Declaration of competing interest

The authors declare that they have no known competing financial interests or personal relationships that could have appeared to influence the work reported in this paper.

Data availability

Data will be made available on request.

Acknowledgement

This study was carried out within the framework of the Deutsche Forschungsgemeinschaft funded research unit RU 2179 "MAD Soil – Microaggregates: Formation and turnover of the structural building blocks of soils" (DFG RU 2179) under the project 251268514.

Appendix A. Supplementary data

Supplementary data to this article can be found online at https://doi.org/10.1016/j.jcis.2024.04.080.

References

[1] M.T. Jorgenson, T.E. Osterkamp, Response of boreal ecosystems to varying modes of permafrost degradation, Can. J. For. Res. 35 (2005) 2100–2111, https://doi.org/10.1139/x05-153.
[2] M. Köchy, R. Hiederer, A. Freibauer, Global distribution of soil organic carbon part 1: masses and frequency distributions of SOC stocks for the tropics, permafrost regions, wetlands, and the world, SOIL 1 (2015) 351–365, https://doi.org/10.5194/soil-1-351-2015.
[3] E. Yergeau, G.A. Kowalchuk, Responses of antarctic soil microbial communities and associated functions to temperature and freeze–thaw cycle frequency, Environ. Microbiol. 10 (2008) 2223–2235, https://doi.org/10.1111/j.1462-2920.2008.
[4] O.S. Pokrovsky, J. Karlsson, R. Giesler, Freeze-thaw cycles of arctic thaw ponds remove colloidal metals and generate low-molecular-weight organic matter, Biogeochemistry 137 (2018) 321–336, https://doi.org/10.1007/s10533-018-0421-6.
[5] Z. Zhang, W. Ma, W. Feng, D. Xiao, X. Hou, Reconstruction of soil particle composition during freeze-thaw cycling: a review, Pedosphere 26 (2016) 167–179, https://doi.org/10.1016/S1002-0160(15)60033-9.
[6] E.C. Rooney, V.L. Bailey, K.F. Patel, M. Dragila, A.K. Battu, A.C. Buchko, A. C. Gallo, J. Hatten, A.R. Possinger, Q. Qafoku, L.R. Reno, M. SanClements, T. Varga, R.A. Lybrand, Soil pore network response to freeze-thaw cycles in permafrost aggregates, Geoderma 411 (2022) 115674, https://doi.org/10.1016/j.geoderma.2021.115674.
[7] S. Christensen, B.T. Christensen, Organic matter available for denitrification in different soil fractions: effect of freeze/thaw cycles and straw disposal, J. Soil Sci. 42 (1991) 637–647, https://doi.org/10.1111/j.1365-2389.1991.tb00110.x.
[8] C.B. Fuss, C.T. Driscoll, P.M. Groffman, J.L. Campbell, L.M. Christenson, T. J. Fahey, M.C. Fisk, M.J. Mitchell, P.H. Templer, J. Duran, J.L. Morse, Nitrate and dissolved organic carbon mobilization in response to soil freezing variability, Biogeochemistry 131 (2016) 35–47, https://doi.org/10.1007/s10533-016-0262-0.
[9] T. Skogland, S. Lomeland, J. Goksøyr, Respiratory burst after freezing and thawing of soil: experiments with soil bacteria, Soil Biol. Biochem. 20 (1988) 851–856, https://doi.org/10.1016/0038-0717(88)90092-2.
[10] J. Attwater, A. Wochner, V.B. Pinheiro, A. Coulson, P. Holliger, Ice as a protocellular medium for RNA replication, Nat. Commun. 1 (2010), https://doi.org/10.1038/ncomms1076.
[11] H. Trinks, W. Schroder, C.K. Biebricher, Ice and the origin of life, Orig. Life Evol. Biosph. 35 (2005) 429–445, https://doi.org/10.1007/s11084-005-5009-1.
[12] S. Deville, Freezing colloids: observations, principles, control, and use, Springer (2017), https://doi.org/10.1007/978-3-319-50515-2.
[13] T. Vajda, Cryo-bioorganic chemistry: molecular interactions at low temperature, Cell. Mol. Life Sci. 56 (1999) 398–414, https://doi.org/10.1007/s000180050441.
[14] H. Liu, Y. Hu, Y. Hao, X. Yan, L. Wu, C. Wang, X. Li, Progressive freeze-thaw redistributes water, solute and CO_2 emissions across soil layers – The role of soil particle size, Catena 219 (2022) 106614, https://doi.org/10.1016/j.catena.2022.106614.
[15] T. Kubo, H. Nakata, T. Kato, Effects of insoluble particles on grain growth in polycrystalline ice: implications for rheology of ice shells of icy satellites, J. Mineral. Petrol. Sci. 104 (2009) 301–306, https://doi.org/10.2465/jmps.090622e.

[16] P.R.F. Barnes, E.W. Wolff, Distribution of soluble impurities in cold glacial ice, J. Glaciol. 50 (2004) 311–324, https://doi.org/10.3189/172756504781829918.
[17] P.B. Price, A habitat for psychrophiles in deep antarctic ice, Proc. Natl. Acad. Sci. 97 (2000) 1247–1251, https://doi.org/10.1073/pnas.97.3.1247.
[18] D.C. Steytler, B.H. Robinson, J. Eastoe, K. Ibel, J.C. Dore, I. MacDonald, Effects of solidification of the oil phase on the structure of colloidal dispersions in cyclohexane, Langmuir 9 (1993) 903–911, https://doi.org/10.1021/la00028a006.
[19] G.M. Marion, Freeze-thaw processes and soil chemistry. US Army corps of engineers cold regions research & engineering laboratory, Technical Report 95–12 (1995). https://apps.dtic.mil/sti/pdfs/ADA295688.pdf.
[20] A. Bogdan, M. Molina, H. Tenhu, E. Bertel, N. Bogdan, T. Loerting, Visualization of freezing process in situ upon cooling and warming of aqueous solutions, Sci. Rep. 4 (2014) 7414, https://doi.org/10.1038/srep07414.
[21] A. Inagawa, T. Ishikawa, T. Kusunoki, S. Ishizaka, M. Harada, T. Otsuka, T. Okada, Viscosity of freeze-concentrated solution confined in micro/nanospace surrounded by ice, J. Phys. Chem. C 121 (2017) 12321–12328, https://doi.org/10.1021/acs.jpcc.7b03792.
[22] C. Belzile, J.A.E. Gibson, W.F. Vincent, Colored dissolved organic matter and dissolved organic carbon exclusion from lake ice: Implications for irradiance transmission and carbon cycling, Limnol. Oceanogr. 47 (2002) 1283–1293, https://doi.org/10.4319/lo.2002.47.5.1283.
[23] T. Bryk, A.D.J. Haymet, Charge separation at the ice/water interface: a molecular dynamics simulation study of solute ions at the ice basal plane, J. Mol. Liq. 112 (2004) 47–50, https://doi.org/10.1016/j.molliq.2003.11.008.
[24] G.W. Gross, The Workman-Reynolds effect and ionic transfer processes at the ice solution interface, J. Geophys. Res. 70 (1965) 2291–2300, https://doi.org/10.1029/JZ070i010p02291.
[25] R.M. Manasypov, S.N. Vorobyev, S.V. Loiko, I.V. Kritzkov, L.S. Shirokova, V. P. Shevchenko, S.N. Kirpotin, S.P. Kulizhsky, L.G. Kolesnichenko, V.A. Zemtzov, V. V. Sinkinov, O.S. Pokrovsky, Seasonal dynamics of organic carbon and metals in thermokarst lakes from the discontinuous permafrost zone of western Siberia, Biogeosciences 12 (2015) 3009–3028, https://doi.org/10.5194/bg-12-3009-2015.
[26] S. Dultz, H. Steinke, R. Mikutta, S.K. Woche, G. Guggenberger, Impact of organic matter types on surface charge and aggregation of goethite, Colloids Surf. A 554 (2018) 156–168, https://doi.org/10.1016/j.colsurfa.2018.06.040.
[27] J.J. Mosher, L.A. Kaplan, D.C. Podgorski, A.M. McKenna, A.G. Marshall, Longitudinal shifts in dissolved organic matter chemogeography and chemodiversity within headwater streams: a river continuum reprise, Biogeochemistry 124 (2015) 371–385, https://doi.org/10.1007/s10533-015-0103-6.
[28] T.E.C. Kraus, R.A. Dahlgren, R.J. Zasoski, Tannins in nutrient dynamics of forest ecosystems - a review, Plant Soil 256 (2003) 41–66, https://doi.org/10.1023/a:1026206511084.
[29] L. Thieme, D. Graeber, D. Hofmann, S. Bischoff, M.T. Schwarz, B. Steffen, U.-N. Meyer, M. Kaupenjohann, W. Wilke, B. Michalzik, J. Siemens, Dissolved organic matter characteristics of deciduous and coniferous forests with variable management: different at the source, aligned in the soil, Biogeosciences 16 (2019) 1411–1432, https://doi.org/10.5194/bg-16-1411-2019.
[30] S. Dultz, R. Mikutta, S.N.M. Kara, S.K. Woche, G. Guggenberger, Effects of solution chemistry on conformation of self-aggregated tannic acid revealed by laser light scattering, Sci. Total Environ. 754 (2021) 142119, https://doi.org/10.1016/j.scitotenv.2020.142119.
[31] K. Walz, Die Bestimmung der Kornform der Zuschlagstoffe, Betonstraße 11 (1936) 27–32.
[32] T. Saruya, K. Nakajima, M. Takata, T. Homma, N. Azuma, K. Goto-Azuma, Effects of microparticles on deformation and microstructural evolution of fine-grained ice, J. Glaciol. 65 (2019) 531–541, https://doi.org/10.1017/jog.2019.29.
[33] R.B. Alley, G.A. Woods, Impurity influence on normal grain growth in the gisp2 ice core, Greenland, J. Glaciol. 42 (1996) 255–260, https://doi.org/10.3189/S0022143000004111.
[34] D.S. Reid, O.R. Fennema, Fennemas Food Chemistry, chapter Water and Ice, 4th edition., CRC Press Boca, Raton, FL, 2007, pp. 17–82.
[35] G. Shao, D.A.H. Hanaor, X. Shen, A. Gurlo, Freeze casting: From low-dimensional building blocks to aligned porous structures—a review of novel materials, methods, and applications, Adv. Mater. 32 (2020) 1907176, https://doi.org/10.1002/adma.201907176.
[36] S. Deville, E. Saiz, R.K. Nalla, A.P. Tomsia, Freezing as a path to build complex composites, Science 311 (2006) 515–518, https://doi.org/10.1126/science.1120937.
[37] V. Riou, A. Vernhet, T. Doco, M. Moutounet, Aggregation of grape seed tannins in model wine—effect of wine polysaccharides, Food Hydrocoll. 16 (2002) 17–23, https://doi.org/10.1016/S0268-005X(01)00034-0.
[38] M. Steiger, Crystal growth in porous materials—I: the crystallization pressure of large crystals, J. Cryst. Growth 282 (2005) 455–469, https://doi.org/10.1016/j.jcrysgro.2005.05.007.
[39] N. Golding, E.M. Schulson, C.E. Renshaw, Shear faulting and localized heating in ice: the influence of confinement, Acta Mater. 58 (2010) 5043–5056, https://doi.org/10.1016/j.actamat.2010.05.040.
[40] R. Sutton, G. Sposito, Molecular structure in soil humic substances: the new view, Environ. Sci. Technol. 39 (2005) 9009–9015, https://doi.org/10.1021/es050778q.
[41] L.-F. Wang, L.-L. Wang, X.-D. Ye, W.-W. Li, X.-M. Ren, G.-P. Sheng, H.-Q. Yu, X.-K. Wang, Coagulation kinetics of humic aggregates in mono- and di-valent electrolyte solutions, Environ. Sci. Technol. 47 (2013) 5042–5049, https://doi.org/10.1021/es304993j.
[42] P. Kolhe, E. Amend, S.K. Singh, Impact of freezing on pH of buffered solutions and consequences for monoclonal antibody aggregation, Biotechnol. Prog. 26 (2010) 727–733, https://doi.org/10.1002/btpr.377.
[43] N. Meiler, R.J. Spencer, J.H. Weare, The prediction of mineral solubilities in natural waters: A chemical equilibrium model for the Na-K-Ca-Mg-Cl-SO_4-H_2O system at temperatures below 25°C, Geochim. Cosmochim. Acta 54 (1990) 575–590, https://doi.org/10.1016/0016-7037(90)90354-N.
[44] N. Kallay, D. Cakara, Reversible charging of the ice–water interface, J. Colloid Interface Sci. 232 (2000) 81–85, https://doi.org/10.1006/jcis.2000.7193.
[45] R.B. Alley, J.H. Perepezko, C.R. Bentley, Grain growth in polar ice: I. theory, J. Glaciol. 32 (1986) 415–424, https://doi.org/10.3189/S0022143000012120.
[46] R.R. Blank, M.A. Fosberg, Effects of freezing on colloidal halloysite: Implications for temperate soils, Clays Clay Miner. 39 (1991) 642–650, https://doi.org/10.1346/CCMN.1991.0390610.
[47] D. Devarajan, L. Liang, B. Gu, S.C. Brooks, J.M. Parks, J.C. Smith, Molecular dynamics simulation of the structures, dynamics, and aggregation of dissolved organic matter, Environ. Sci. Technol. 54 (2020) 13527–13537, https://doi.org/10.1021/acs.est.0c01176.
[48] J. Chen, S. Xue, Y. Lin, C. Wang, Q. Wang, Q. Han, Effect of freezing–thawing on dissolved organic matter in water, Desalination Water Treat. 57 (2015) 17230–17240, https://doi.org/10.1080/19443994.2015.1085913.
[49] S. Xue, Y. Wen, X. Hui, L. Zhang, Z. Zhang, J. Wang, Y. Zhang, The migration and transformation of dissolved organic matter during the freezing processes of water, J. Environ. Sci. 27 (2015) 168–178, https://doi.org/10.1016/j.jes.2014.05.035.
[50] P.E. Kepkay, Particle aggregation and the biological reactivity of colloids, Mar. Ecol. Prog. Ser. 109 (1994) 293, https://doi.org/10.3354/meps109293.
[51] N. Mergelov, V. Targulian, Accumulation of organic matter in the mineral layers of permafrost-affected soils of coastal lowlands in East Siberia, Eurasian Soil Sci. 44 (2011) 249–260, https://doi.org/10.1134/S1064229311030069.
[52] N. Gentsch, R. Mikutta, R.J.E. Alves, J. Bárta, P. Čapek, A. Gittel, G. Hugelius, P. Kuhry, K. Lashchinskiy, J. Palmtag, A. Richter, H. Šantrůčková, J. Schnecker, O. Shibistova, T. Urich, B. Wild, G. Guggenberger, Storage and transformation of organic matter fractions in cryoturbated permafrost soils across the Siberian Arctic, Biogeosciences 14 (2015) 4525–4542, https://doi.org/10.5194/bg-12-4525-2015.
[53] I. Prater, S. Zubrzycki, F. Buegger, L.C. Zoor-Füllgraff, G. Angst, M. Dannenmann, C.W. Mueller, From fibrous plant residues to mineral-associated organic carbon – the fate of organic matter in Arctic permafrost soils, Biogeosciences 17 (2020) 3367–3383, https://doi.org/10.5194/bg-17-3367-2020.